

Chapter 10

Forest Health Monitoring using Hyperspectral Remote Sensing Techniques



Narayan Kayet

Abstract Hyperspectral Remote sensing is a handy tool for forest health monitoring. This study focuses on forest health monitoring using hyperspectral satellite data and validates it with tree spectral data. In the study area, increasing mining and anthropogenic activities within and near forest lands have caused threats to forest health. All these necessitate assessing the forest health in the areas surrounding mines. We have used two methods for the forest health assessment: one is VIs (vegetation indices) based model, and another is tree spectral analysis. The supervised classification (SAM) method was used for forest health classification based on spectral data. The results showed that a healthy forest portion was located in the hilly side of the study area while an unhealthy segment was situated alongside the mines. Hyperspectral data-based VIs model shows better accuracy than spectral based other methods. Also, it was found that the hyperspectral data based forest health classification gave a higher accuracy than multispectral data. Finally, forest health results were justified by ground tree spectral data. This work provides an effective guideline for forest planning and management.

Keywords Forest health · Hyperspectral data · Vegetation indices · GIS · Mining area

10.1 Introduction

Hyperspectral remote sensing is a very useful tool for forest health monitoring. Hyperspectral data are spectrally overdetermined, which means that they provide spectral information to identify and distinguish spectrally unique materials. Also this data has the potential for more accurate information extraction than possible from multispectral data (Apostolescu et al. 2016; Navinkumar and Parmar 2016). The hyperspectral sensor provides hundreds of narrow spectral bands of the Earth's

N. Kayet (✉)

Department of Mining Engineering, Indian Institute of Technology, Kharagpur, India
e-mail: narayankayet@gmail.com

surface features. NASA EO-1 satellite, equipped with the Hyperion spectrometer, which has a sampling distance of 10 nm within the 7.7 km swath path, provides 242 spectral bands within the range of 400–2500 nm wavelengths of the EM spectrum (Hyperion user guide). This sensor easily detects forest biochemical and biophysical properties (Asner et al. 2015; Thenkabail et al. 2001; Chambers et al. 2007). Hyperspectral data can detect pest and blight conditions in a forest as well as be used for assessing areas for timber harvesting. Narrow-banded hyperspectral data has been used for forest health mapping (Tuominen et al. 2009; Kayet et al. 2019a, b), to depict the overall healthy and unhealthy portions of a forest. Recent developments in hyperspectral data acquisition from satellite-borne spectrometers have opened new areas of research that could bring revolutionary changes in the current approaches to forest management (Franklin 2001). Some researchers have worked on vegetation stress from the derivative chlorophyll index and leaf area index (Broge and Leblanc 2001; Brantley et al. 2011; Darvishzadeh et al. 2011). They have used the airborne hyperspectral image for this analysis. Detection of vegetation stress by hyperspectral remote sensing technique is based on the assumption that vegetation stress factors interfere with photosynthesis or the physical structure of the vegetation and affect the absorption of light energy and thus alter the reflectance spectrum of the vegetation (Zarco-Tejada et al. 2009; Jacquemoud et al. 2009; Bellvert et al. 2014). Airborne hyperspectral data is used for the estimate and distribution of different species in the forest areas. Hyperspectral data has used to develop the Photochemical Reflectance Index (PRI) for distinguishing the species-wise variations of leaves (Cho et al. 2008; Mashimbye et al. 2012; Darvishzadeh et al. 2008). The hyperspectral narrow banded data-based NDVI (normalized difference vegetation index) and LAI (leaf area index) has been used for plant health detection by Zarco-Tejada et al. (2005). They had used red, red edge, and NIR bands for this analysis. The International Institute for Geo-Information Science and Earth Observation (ITC) has studied vegetation health and tree species classification using hyperspectral data. They have used full pixel classification methods for vegetation health and tree species based on ground tree spectral data (Vauhkonen et al. 2011; Dalponte et al. 2014). The decision tree classifier tool of ENVI will be used to classify the pixels of a Hyperion image for necessary information acquisition for forest management purposes (vegetation indices tutorial ENVI). Ma et al. (2017) used airborne Hyperspectral data to develop photochemical reflectance index (PRI) for distinguishing the species wise variations of leafs. A number of researchers have assessed the vegetation stress from derivative chlorophyll index and leaf area index estimation, using compact airborne spectrographic image (Wu et al. 2010; Zarco-Tejada et al. 2002; Lee et al. 2004). The detection of vegetation stress by hyperspectral remote sensing techniques is based on the assumption that vegetation stress factors interfere with photosynthesis or the physical structure of the vegetation and affect the absorption of light energy and thus alter the reflectance spectrum of vegetation (Zarco-Tejada et al. 2009; Calderon et al. 2013; Li and Guo 2016).

The study area is located in the in an region that has many mines. Mining fields are under high-stress conditions showing signs of dry and dying plant species. In the study area, increasing mining and anthropogenic activities within and near forests pose threats to forest health. All these necessitate monitoring of the forest health in surrounding mining areas.

10.2 Materials and Methods

10.2.1 Study Area

The present study has been done in the Saranda Forest and its surrounding areas, which are located in the West Singhbhum district of the Indian state of Jharkhand (Fig. 10.1). It is famous for having Asia’s largest Sal forests and is an important elephant habitat. Over the last few decades, in this region, many iron ore mining towns have emerged, e.g. Gua, Chiria, Megataburu and Kiriburu. The Saranda forest of Jharkhand is endowed with some rich iron ore deposits. The location of the forest is within latitude $22^{\circ} 3' 7.98'' - 22^{\circ} 14' 0.67''$ N and longitude $85^{\circ} 21' 31.52'' - 85^{\circ} 25' 53.18''$ E with elevation of 850 m above the mean sea level (MSL). Saranda forest is fed by two major rivers, Karo and Koina. The catchment of these rivers comprises of a drainage system with stream order of up to six (Kayet et al. 2016).

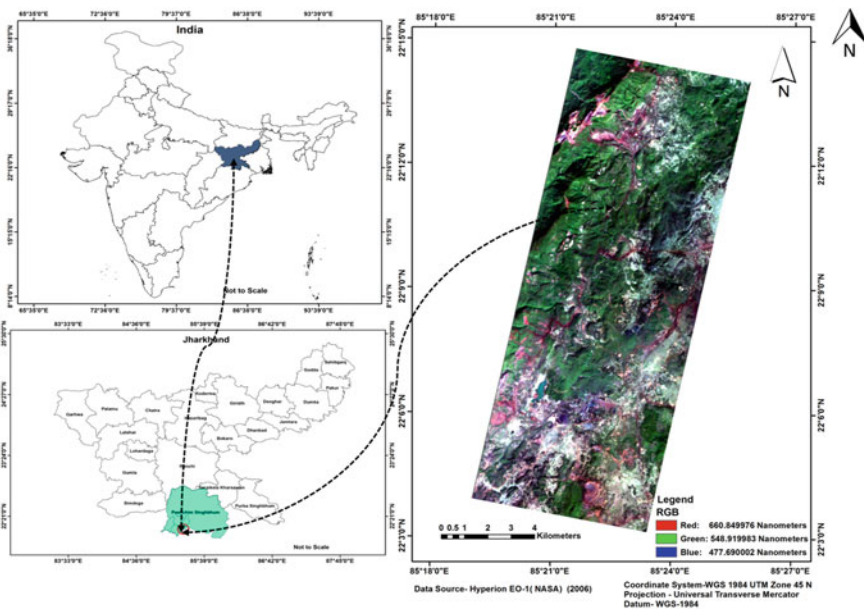


Fig. 10.1 Location map of the study area



Fig. 10.2 Trees spectral data collected from field

10.2.2 Data Source

Hyperspectral data (Hyperion) were downloaded from the USGS website and used for forest health monitoring. Healthy and unhealthy tree spectra data were collected by a field spectroradiometer instrument. Also, healthy and unhealthy forest locations (latitude and longitude) were recorded by GPS. Photographs are taken for validation purposes during the field survey (Fig. 10.2).

10.2.3 Data Pre-processing

Bad bands removal: The delivered USGS Hyperion product level L1R has 242 bands, of which 44 were not calibrated. The main reason for not calibrating the entire band was the decreased sensitivity of the detectors within the non-calibrated spectral regions. Out of the total collected 242 Hyperion bands, 44 (Table 10.1) bands do not work (Han et al. 2002).

De-stripping: Hyperion L1R data shows a severe striping effect by imprecise co-calibration of individual detectors on the focal plane array. The first 12 visible near-infrared bands and many short waves infrared bands are affected by striping and

Table: 10.1 List of unused bands of the hyperion sensor

Bands	Description
1–7	Not illuminated
58–78	Overlap region
120–132	Water vapour absorption Band
165–182	Water vapour absorption band
185–187	Identified by hyperion bad band list
221–224	Water vapour absorption Band
225–242	Not illuminated

bad columns. An uncorrected striping effect will lead to a faulty interpretation of the results. The vertical stripes error values were replaced by the average DN values of the adjacent columns. Hyperspectral data are affected by different noise sources which can be grouped into two main classes: random noise and fixed pattern noise. The photon and thermal noise are random noise; striping noise is a fixed pattern noise and created from push-broom sensors. Hyperspectral images are affected by those noises. Geometric correction: Geometric distortion often has to be removed from remotely sensed data. There are two main approaches to remove the geometric errors. One is the systematic approach and the other is the non-systematic approach. Some of these errors can be corrected by using the ephemeris of the platform and previously known internal sensor distortion characteristics. Other errors can be rectified by matching image coordinates of physical features recorded by the image to the geographic coordinates of the same feature collected from a map or by using a Global Positioning System (GPS).

Radiometric correction: Cross-track illumination- ENVI cross-track illumination tool was used to remove variation of illumination of the image. Cross-track illumination errors may be due to vegetating effects, instrument effects or scanning or other non-uniform illumination effects. The EFFORT algorithm calculates the mean values of an extended track polynomial function, and fit mean values remove this error. We have used this algorithm to remove the variation of illumination of the image.

Atmospheric correction (FLAASH): Atmospheric correction reduces the effects of the atmospheric components (water vapor, dust, gasses) on the electromagnetic radiation reflected or emitted from the surface. We have used the FLAASH model (Fast Line-of-sight Atmospheric Analysis of Spectral Hypercubes) in ENVI software for atmospheric correction and convert to surface reflectance. This model was developed by Spectral Sciences, Inc., under the sponsorship of the US Air force Research Lab. The calibration model based on the theory of atmospheric radiation is according to the physical process of radiation transfer, building by radiation transfer equation, using a theoretical formula (Cooley et al., 2002) to proceed with atmospheric correction (Eq 1).

$$L = \left(\frac{Ap}{1 - peS} \right) + \left(\frac{Bpe}{1 - pes} \right) + La$$

$$Le = \left(\frac{(A + B)pe}{1 - peS} \right) + La$$

FLAASH starts from a standard equation for spectral radiance at a sensor pixel, L ; that applies to the solar wavelength range and flat, Lambert a material or their equivalents. FLAASH atmospheric correction removes this absorption feature. FLAASH MODTRAN has outperformed other radiative transfer codes especially in the water region 940 and 1130 nm and CO₂ at 2055 nm (Pathak et al. 2016).

10.2.4 Methodology

10.2.4.1 Vegetation Indices (Vis)-Based Forest Health Mapping

The forest health analysis tool will generate a spatial map that shows the overall health and vigor of a forested area (Tuominen et al. 2008). It is good at detecting pest and blight conditions in a forest. The forest health tool uses the following vegetation index categories (ENVI Forest health tutorial):

1. Narrow band Greenness, to show the distribution of green.
2. Leaf pigments, to show the concentration of aryteneoids and anthocyanin pigments for stress levels.
3. Canopy water content, to show the concentration of water.
4. Light use efficiency, to show forest growth rate.

Greenness indices: Greenness vegetation indices generally measure the vigor and green vegetation (Kumar et al. 2015). They measure the various aspects such as chlorophyll concentration, canopy area, and canopy structure. Greenness vegetation indices are based on measuring the reflectance peak in the NIR region. Red wavelengths where the chlorophyll absorption is strongest are used as a reference (Lloret et al. 2004). **Leaf pigments indices:** Leaf pigment vegetation indices measure the amount of stress-related pigment in the vegetation (Jenkins et al. 2007). In stressed vegetation, there is a higher concentration of carotenoids and anthocyanins. Carotenoids are the leaf's pigment that prevents vegetation light conditions. Anthocyanin pigment contents are high in new leaves (Gamon et al. 1999). **Canopy water content indices:** Water content vegetation indices are designed to estimate the canopy water content (Colombo et al. 2008). However, water content is an important vegetation property that controls vegetation growth and also correlates with vegetation health (Adam et al. 2010). The use of water content vegetation indices needs high spectral resolution data.

Table 10.2 Narrow banded VIs for forest health mapping

Narrow banded Indices	Indices	Algorithms	References
Greenness	(i) Modified red edge normalized difference vegetation index (ii) Vogelmann red edge index	$mNDVI705 = (750nm\ 705nm)/(750nm + 705nm (2 * 445nm))$ $VREI1 = 740nm/720nm$	Datt (1999), Zarco-Tejada et al. (2013)
Light use efficiency	Structure insensitive pigment index	$SIPI = (800nm - 445nm)/(800nm - 680nm)$	Penuelas et al. (1994)
Leaf pigments	(i) Carotenoid reflectance index (ii) Anthocyanin reflectance index	$ARI1 = \frac{1}{550nm} - \frac{1}{700nm}$ $CR12 = (1/510nm)(1/550nm)$	Gitelson et al. (2002)
Canopy water content	Normalized difference infrared index	$NDII = 819nm - 1649nm/819nm - 1649nm$	Hardisky et al. (1983)

Light Use Efficiency indices: Light use efficiency vegetation indices provide the efficiency with which vegetation can use incident light for photosynthesis (Wilson et al. 1981). It is correlated with carbon uptake efficiency and growth rate. However, by the use of light use efficiency vegetation indices measure the growth rate and production of vegetation. We have used six narrow banded VIs for forest health mapping (Table 10.2).

10.2.4.2 Spectral Analysis Based Forest Health Mapping

The following procedures of Hyperspectral analysis were employed, including the Minimum Noise Fraction (MNF) transformation for reducing the spectral data, the Pixel Purity Index (PPI) for identifying those extreme or spectrally pure pixels, and the n-dimensional visualizer for determining the endmember directly from the image. Spectral Angle Mapper (SAM) was applied to estimate the abundances of each endmember to produce the final map.

Minimum Noise Fraction (MNF): MNF can reduce the inherent dimensionality of the dataset and reduce noise from the dataset. MNF also reduces the computational requirement for subsequent processing. The first step in MNF transforms the

data in which the noise has a unit variance and there is also no band to band inter-relationship (Denghui and Le 2011). Secondly, the MNF can compute/process the principal component analysis for noise-whitened data (Gamon et al. 2004). MNF inversion produces much smaller spectral angles than those derived in transformed space (Peddle et al. 2008). The first ten inverse MNF bands contain 95% of the total information.

Pixel purity index (PPI): Image transformation techniques typically use statistical analysis and reduce the dimensionality of the data. One such transformation is done through the principal component analysis or principal component transformation (Chang and Plaza 2006). The pixel purity index (PPI) is a means of finding the most spectrally pure, or extreme, pixels in multispectral and hyperspectral images (Chaudhry et al. 2006). The most spectrally pure pixels typically correspond to mixing endmembers (Plaza et al. 2006).

N-dimensional (N-D) Visualizer: N-D is applied after correcting the image. The distribution of bands in N space can be used for the estimation of some spectral endmembers and their pure spectral signature (Kruse et al. 1999). The N-dimensional visualization is applied after gathering the data through MNF or PPI algorithms. The pre-clustering result attempts to find in the corner pixel of N-dimensional using a spectral scatter algorithm.

Since the purest pixel is found in the neighbourhood of the data cloud (Wang et al. 2015). The n-dimensional visualizer allows for the interactive rotation of data in n-D space, selection of groups into different classes (Boardman et al. 1995).

Spectral classification techniques: Classification and feature extraction methods have been commonly used for many years for the mapping of forest health and vegetative cover from hyperspectral datasets. However, conventional classification algorithms cannot be applied to hyperspectral data due to the high dimensionality of the data. Spectral Angle Mapper (SAM) mapping techniques were used in the present study to map of forest health in the study area. Spectral Angle Mapper (SAM) is an algorithm, which is widely used for hyperspectral image correction (Petropoulos et al. 2013). It is a supervised image correction process. A pixel with a minimum spectral angle comparison with reference spectra is assigned to the pixel vector. This algorithm determines the spectral similarity between two spectra by calculating the angle between the spectra and treating them as vectors in space with dimensionality equal to the number of bands (Girouard et al. 2004).

10.2.4.3 Accuracy Assessment

Accuracy assessment is an important work in the classification validation system. Remote sensing technology is a great source of thematic map presentation although accuracy assessment assists how far the classification represents the real world. Accuracy assessment can produce user accuracy, producer accuracy, total accuracy, and also kappa coefficient value.

The producer accuracy of the classified pixels compared to the ground truth. The overall research methodology is shown in Fig. 10.3.

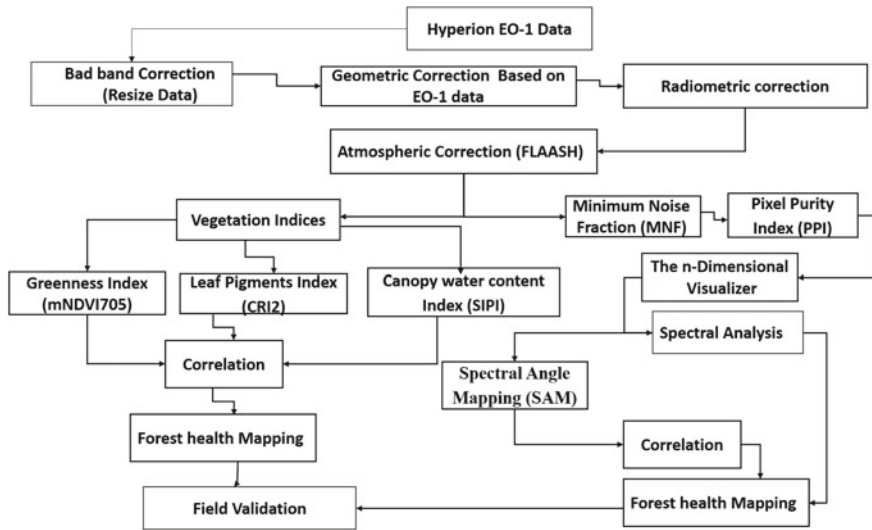


Fig. 10.3 Overall methodology for forest health monitoring

Table 10.3 Minimum, maximum, mean, and standard deviation values of before and after FLAASH correction

FLAASH correction	Min	Max	Mean	Stdev
Before correction	-77	3383	84,444.44	66,423.37
After correction	0	70.89	11.63	10.21

10.3 Results and Discussion

10.3.1 Result of FLAASH Atmospheric Correction

FLAASH is an effective atmospheric correction process where all bands are corrected to follow their proper geometric and radiometric characteristics. FLAASH can also remove the de-stripping of the image, path radiation of the image, and various systematic and non-systemic effects. Pre and post FLAASH correction statistics value are shown in Table 10.3. Spectral variability of after FLAASH correction is shown in Fig. 10.4.

10.3.2 Vegetation Indices (Vis) Based Forest Health Mapping

Vegetation Indices (VIs) were calculated for 60 test sample pixels. Mean and standard deviation values for both healthy and unhealthy classes are shown in Table 10.4.

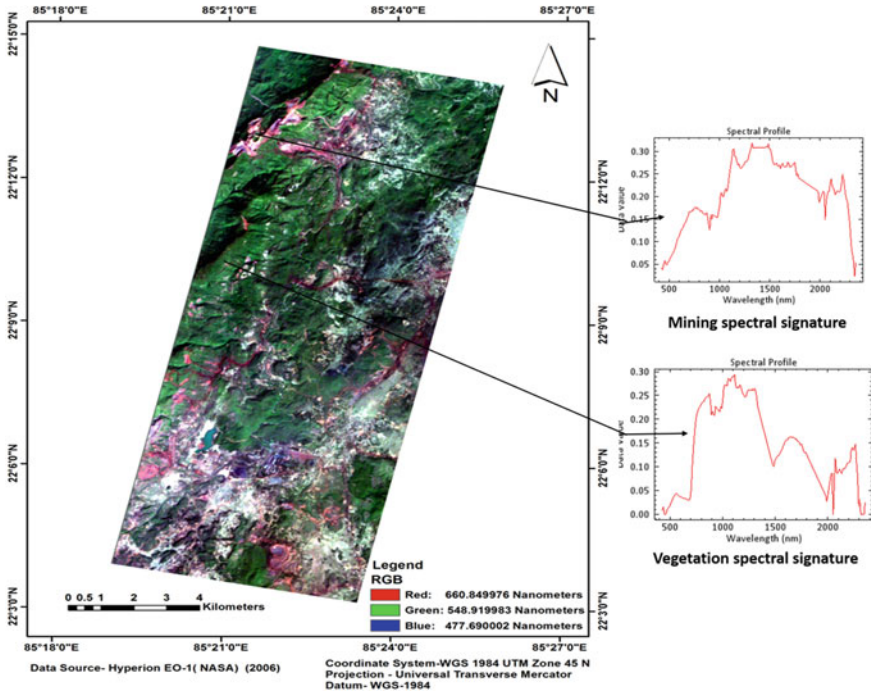


Fig. 10.4 Image spectra after atmospheric correction

Table 10.4 Mean, standard deviation and separability values for each index test

Vegetation indices	Healthy		Unhealthy		Separability S
	Mean	Std.	Mean	Std.	
MNDVI705	0.66	0.03	0.17	0.08	4.21
VREI1	1.44	1.13	0.06	0.05	2.60
CRI1	33.22	7.92	17.17	2.24	1.57
ARI1	9.65	4.78	7.71	2.29	0.27
NDII	-0.49	0.07	-1.23	0.27	2.11
SIPI	1.09	0.02	0.51	0.33	1.60

Generally, the separability values obtained for greenness and vegetation indices were relatively high. The highest separability values were obtained for the modified red edge normalized difference vegetation (MNDVI705) index due to good chlorophyll content. The MNDVI705 correlates well with good chlorophyll content, so its good performance could be expected as the result of forest health (Kayet et al. 2019a, b). ENVI software provides nine forest health classes (Fig. 10.5).

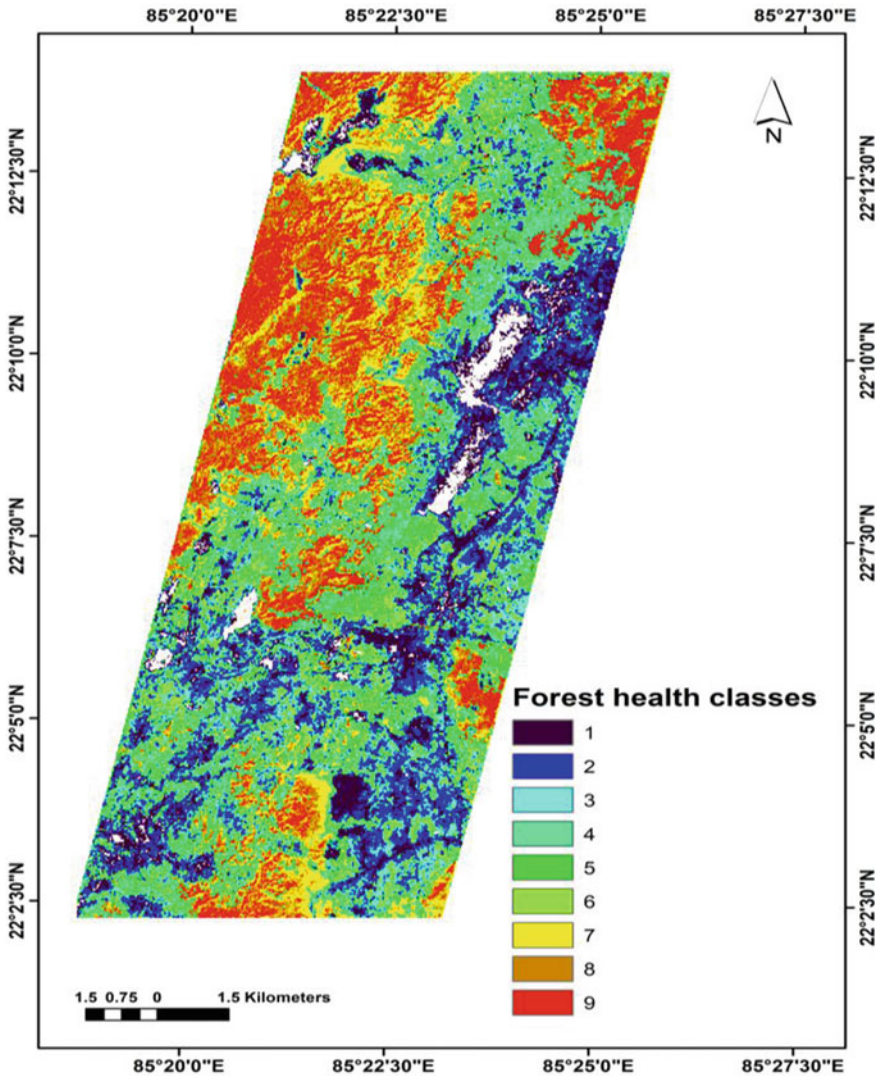


Fig. 10.5 Forest health map (Class 9 very healthy and class 1 unhealthy)

The classifications are relative to the particular input scene only and cannot be generalized to other areas or other scenes. The healthy and unhealthy value range is 0.5–0.8 and 0.1–0.3 (Kayet et al. 2019a, b). The classification map rates the scene from one, representing the least healthy forest (weakest) to the healthiest forest (strongest) which help to assess relative forest health conditions within the scene (ENVI forest health tool tutorial).

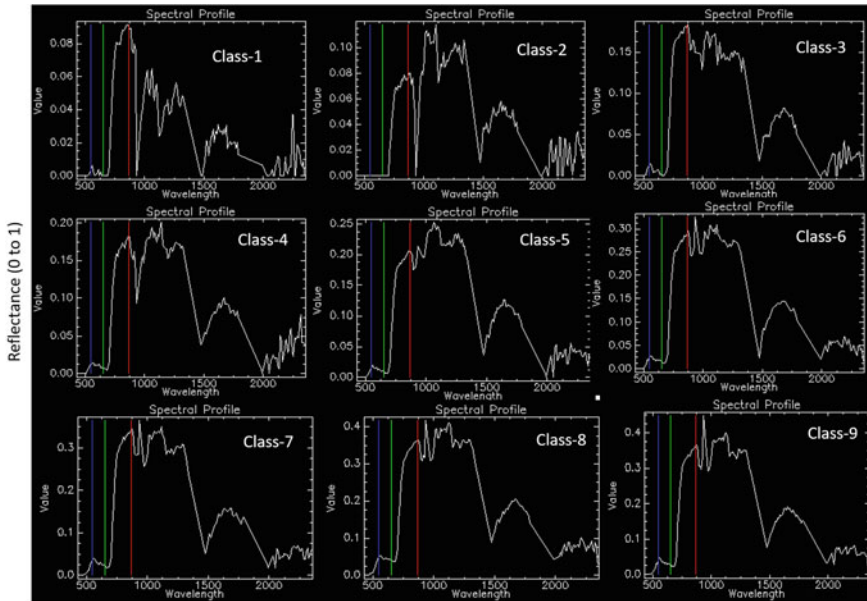


Fig. 10.6 Hyperion reflectance spectra of forest health classes (1–9)

Forest health classification was done by the use of three narrow-band vegetation indices which are MNDVI705 (Greenness or chlorophyll vegetation Index), CRI_1 (Leaf pigment Vegetation Index), and SIPI (Light efficiency vegetation Index). The MNDVI705 index works well with the lower chlorophyll content, so it is accepted for appreciable forest health result (Kumar et al. 2015). Test of forest health result for leaf pigments VIs is relatively lower than any other vegetation indices. In leaf pigment VIs, the value of ARI1 is high than other VIs (Serrano et al., 2002). For light use efficiency, Vis value is relatively higher than that of leaf pigment VIs (Jenkins et al. 2007). NDNI is a useful index where there exhibits a high variability in canopy or leaf pigment structure (Rodriguez et al. 2007). The test result for canopy water content index was low because of vegetation canopy structure (Sims et al. 2002). The Hyperion spectral signature of each forest health class is shown in Fig. 10.6.

10.3.3 Spectral Analysis Based Forest Health Mapping

Forest health is mainly dependent on various physiological parameters such as climate, temperature, geology, soil, slope, aspect, hill shade direction, and much more. The study area is mainly covered by three types of forest health (healthy, moderated healthy, and unhealthy). The healthy and unhealthy value range is 0.5–0.8 and 0.1–0.3 (Kayet et al. 2019a, b). The spectral signature of the forest health

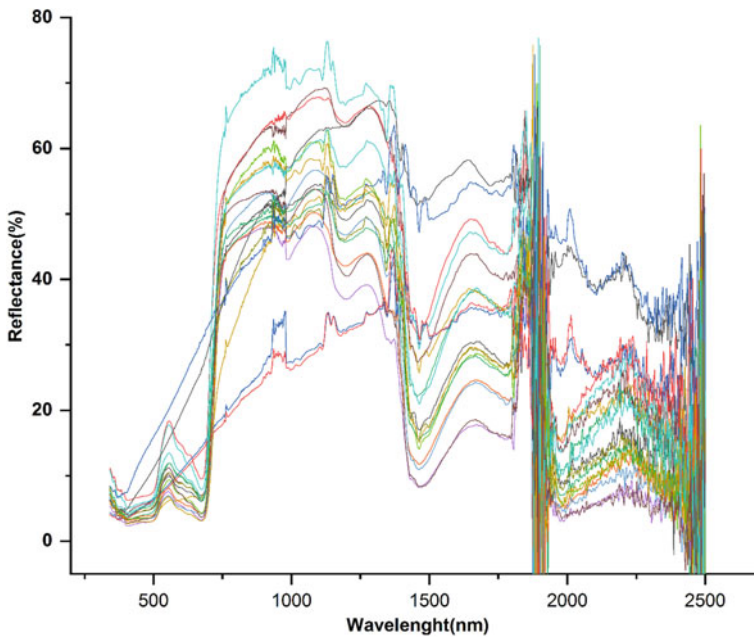


Fig. 10.7 Field collected healthy and unhealthy trees spectra

classes were collected from the image and these match the spectral signature from field collected tree spectral library (Fig. 10.7) and field sample data in ENVI software.

Forest health mapping is done by the SAM classification technique. Classification of forest health into three classes (healthy, moderated healthy, and unhealthy) is shown in Fig. 10.8.

Healthy forest (0.5–0.8) cover comprises 49.87% of the study area, 14.15% area is covered by moderate healthy forest (0.3–0.5), and unhealthy forest (0.1–0.3) covers 38.03% area (Kayet et al. 2019a, b). Healthy forests are present mostly in the north and the north-east part of the study area and unhealthy is situated in mines surrounding area. George et al. (2014) shown the better forest classification through Hyperspectral remote sensing and compared the classification results obtained from Hyperion and Landsat TM sensors for the study of Western Himalaya and obtained collective accuracies of 81.52% and 69.62% respectively. Thenkabail et al. (2004) compared the classification results of different sensors viz., Hyperion, IKONOS, ALI, and ETM + sensors for the study of African rainforests and obtained collective accuracies of 93.2%, 87.46%, 81.53%, and 76.9% respectively.

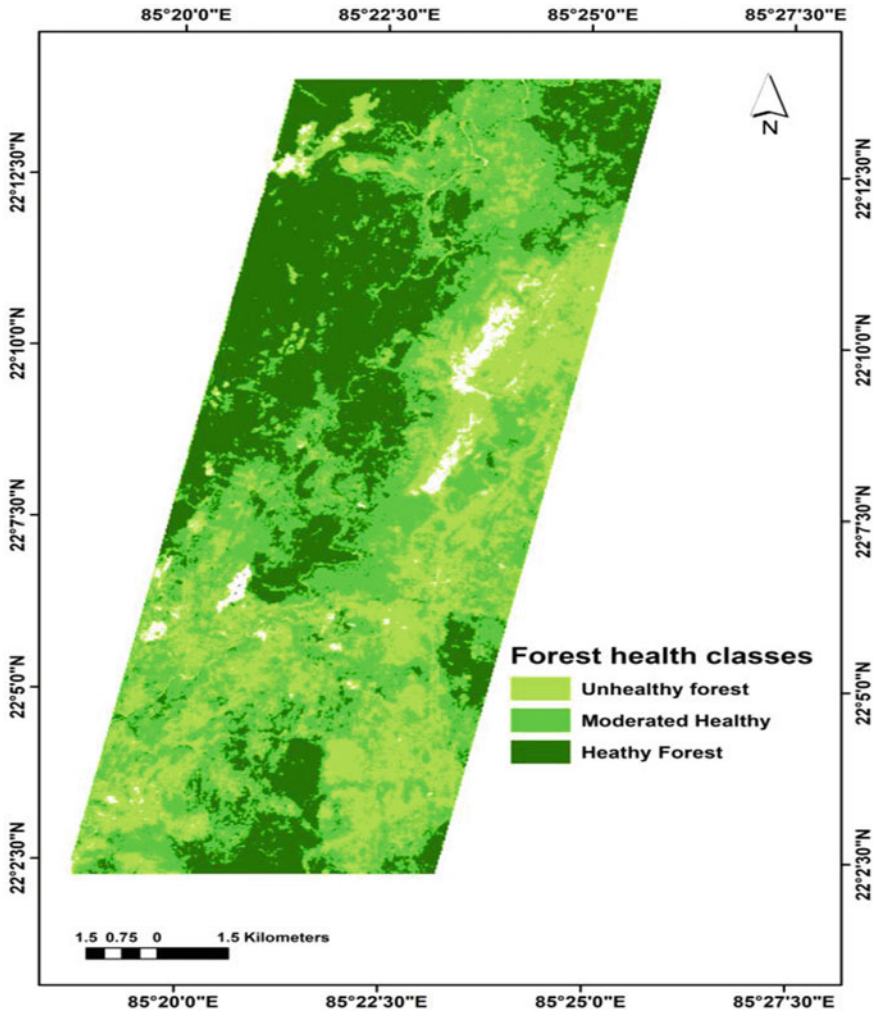


Fig. 10.8 Forest health mapping by hyperion data

10.3.4 Accuracy Assessment

Classification accuracy was done by spectral angle mapper (SAM) classification technique in ENVI software. SAM was implemented to the collection of the spectral signature of healthy, moderated healthy and unhealthy forests. Forest health classification is accuracy by the USGS spectral library and sample field points. Thus, the overall accuracy of 76.53% and 0.71 kappa coefficient were determined (Table 10.5).

Table 10.5 Accuracy assessment results of SAM based on hyperion data

SVM based on hyperion	Healthy	Moderated healthy	Unhealthy	Total	UA
Healthy	11	0	1	11	81.52
Moderated healthy	0	13	0	13	74.54
Unhealthy	2	0	10	12	70.66
Total	13	13	11	36	
PA	91.83	85.53	80.11		

Overall accuracy: 76.53%, kappa statistics: 0.71

10.3.5 Forest Health Validation

The healthy, moderately healthy, and unhealthy components constituting the forest of the study area were evaluated, both at ground level and pixel- level, having the highest reflectance data from the NIR wavebands region. The correlation determination (R^2) and RMS error values were evaluated from ground level and pixel-level spectral data (Fig. 10.9). A correlation ($R^2 = 0.84$) was observed between the ground level and

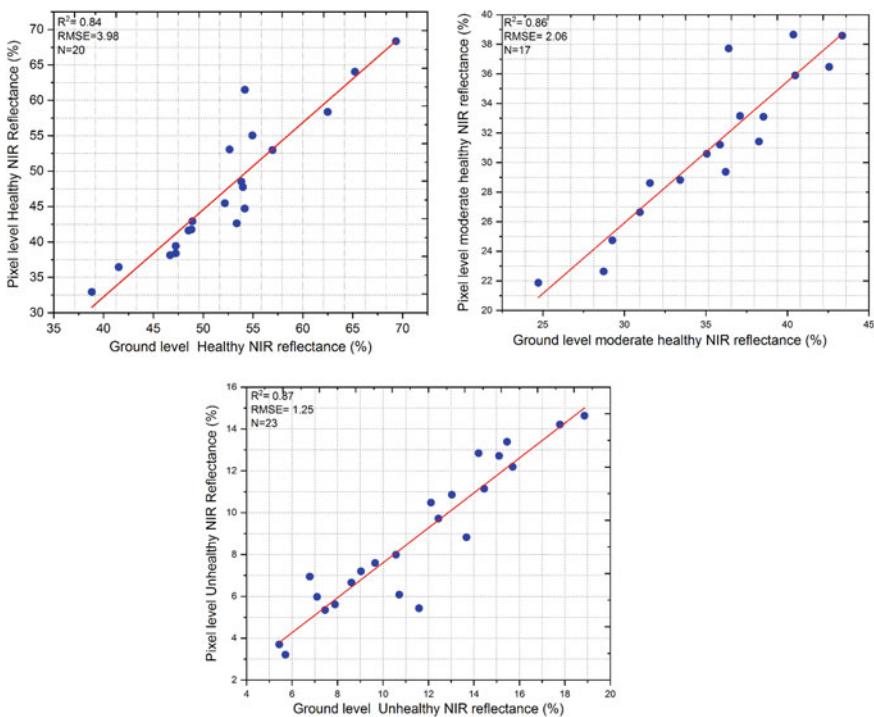


Fig. 10.9 Correlation between field reflected spectra and pixel reflected spectra of healthy, moderate healthy and unhealthy forest class

pixel-level for class healthy, and an RMS error of 3.98 was found. A correlation ($R^2 = 0.86$) was observed between the ground level and pixel-level for class moderately healthy, and an RMS error of 2.06 was found. And a correlation ($R^2 = 0.87$) was observed between the ground level and pixel-level for class unhealthy, and an RMS error of 1.25 was found.

10.4 Conclusion

The article has summarized forest health monitoring sounding mines areas. This case study demonstrated by hyperspectral data. Hyperspectral data has more capability than multispectral data. In this study, a good correlation was shown between forest health and distance from mines. It means that as the mining area increases forest as well as environment will also get affected. This methodology would be capable of monitoring various categories of forest region routinely irrespective of the different climate condition, forest structure, and soil condition. Hyperspectral remote sensing-based forest health monitoring is today's need so that the forest department, local self-government, and mining companies must adopt an adequate policy for reclamation and restoration of the forest ecosystem affected by mining activities.

References

- Adam E, Mutanga O, Rugege D (2010) Multispectral and hyperspectral remote sensing for identification and mapping of wetland vegetation: a review. *Wetlands Ecol Manage* 18(3):281–296
- Apostolescu N, Baran D (2016) Spectral similarity in hyperspectral image. *Acta Electrotechnica* 57
- Asner GP, Ustin SL, Townsend PA, Martin RE, Chadwick KD (2015) Forest biophysical and biochemical properties from hyperspectral and LiDAR remote sensing. *Land resources monitoring, modeling and mapping with remote sensing*. CRC Press, Taylor & Francis Group, pp 429–448.
- Bellvert J, Zarco-Tejada PJ, Girona J, Fereres EJPA (2014) Mapping crop water stress index in a 'Pinot-noir' vineyard: comparing ground measurements with thermal remote sensing imagery from an unmanned aerial vehicle. *Precision Agric* 15(4):361–376
- Boardman JW (1995) Analysis, understanding, and visualization of hyperspectral data as convex sets in n space. In: *Imaging spectrometry* (vol 2480). International Society for Optics and Photonics, pp 14–22
- Brantley ST, Zinnert JC, Young DR (2011) Application of hyperspectral vegetation indices to detect variations in high leaf area index temperate shrub thicket canopies. *Remote Sens Environ* 115(2):514–523
- Broge NH, Leblanc E (2001) Comparing prediction power and stability of broadband and hyperspectral vegetation indices for estimation of green leaf area index and canopy chlorophyll density. *Remote Sens Environ* 76(2):156–172
- Calderón R, Navas-Cortés JA, Lucena C, Zarco-Tejada PJ (2013) High-resolution airborne hyperspectral and thermal imagery for early detection of *Verticillium* wilt of olive using fluorescence, temperature and narrow-band spectral indices. *Remote Sens Environ* 139:231–245

- Chambers JQ, Asner GP, Morton DC, Anderson L, O, Saatchi SS, Espirito-Santo FD, Souza, C Jr. (2007) Regional ecosystem structure and function: ecological insights from remote sensing of tropical forests. *Trends Ecol Evolut* 22(8):414–423
- Chang CI, Plaza A (2006) A fast iterative algorithm for implementation of pixel purity index. *IEEE Geosci Remote Sens Lett* 3(1):63–67
- Chaudhry F, Wu CC, Liu W, Chang CI, Plaza A (2006) Pixel purity index-based algorithms for endmember extraction from hyperspectral imagery. *Recent Adv Hyperspect Signal Image Process* 37(2):29–62
- Cho MA, Sobhan I, Skidmore AK, De Leeuw J (2008) Discriminating species using hyperspectral indices at leaf and canopy scales. *The International Archives of the Spatial Information Sciences*, pp 369–376
- Colombo R, Meroni M, Marchesi A, Busetto L, Rossini M, Giardino C, Panigada C (2008) Estimation of leaf and canopy water content in poplar plantations by means of hyperspectral indices and inverse modeling. *Remote Sens Environ* 112(4):1820–1834
- Cooley T, Anderson GP, Felde GW, Hoke ML, Ratkowski AJ, Chetwynd JH, Bernstein LS (2002, June) FLAASH, a MODTRAN4-based atmospheric correction algorithm, its application and validation. In: *IEEE International Geoscience and Remote Sensing Symposium*, Vol 3. IEEE, pp 1414–1418
- Dalponte M, Ørka HO, Ene LT, Gobakken T, Næsset E (2014) Tree crown delineation and tree species classification in boreal forests using hyperspectral and ALS data. *Remote Sens Environ* 140:306–317
- Datt B (1999) Remote sensing of water content in Eucalyptus leaves. *Aust J Bot* 47(6):909–923
- Darvishzadeh R, Atzberger C, Skidmore A, Schlerf M (2011) Mapping grassland leaf area index with airborne hyperspectral imagery: a comparison study of statistical approaches and inversion of radiative transfer models. *ISPRS J Photogram Remote Sens* 66(6):894–906
- Darvishzadeh R, Skidmore A, Schlerf M, Atzberger C, Corsi F, Cho M (2008) LAI and chlorophyll estimation for a heterogeneous grassland using hyperspectral measurements. *ISPRS J Photogram Remote Sens* 63(4):409–426
- Denghui Z, Le Y (2011) Support vector machine based classification for hyperspectral remote sensing images after minimum noise fraction rotation transformation. In: *2011 International conference on internet computing and information services*. IEEE, pp 132–135
- Franklin SE (2001) Remote sensing for sustainable forest management. CRC press
- Gamon JA, Surfus JS (1999) Assessing leaf pigment content and activity with a reflectometer. *The New Phytol* 143(1):105–117
- Gamon JA, Huemmrich KF, Peddle DR, Chen J, Fuentes D, Hall FG, Miller JR (2004) Remote sensing in BOREAS: Lessons learned. *Remote Sens Environ* 89(2):139–162
- George R, Padalia H, Kushwaha SPS (2014) Forest tree species discrimination in western Himalaya using EO-1 Hyperion. *Int J Appl Earth Obs Geoinf* 28:140–149
- Girouard G, Bannari A, El Harti A, Desrochers A (2004) Validated spectral angle mapper algorithm for geological mapping: comparative study between QuickBird and landsat-TM. In: *XXth ISPRS congress, geo-imagery bridging continents*, Istanbul, Turkey, pp 12–23
- Gitelson AA, Stark R, Grits U, Rundquist D, Kaufman Y, Derry D (2002) Vegetation and soil lines in visible spectral space: a concept and technique for remote estimation of vegetation fraction. *Int J Remote Sens* 23(13):2537–2562
- Han T, Goodenough DG, Dyk A, Love J (2002) Detection and correction of abnormal pixels in Hyperion images. In: *IEEE international geoscience and remote sensing symposium*, vol 3. IEEE, pp 1327–1330
- Jacquemoud S, Verhoef W, Baret F, Bacour C, Zarco-Tejada PJ, Asner GP, Ustin SL (2009) PROSPECT+SAIL models: a review of use for vegetation characterization. *Remote Sens Environ* 113:S56–S66
- Jenkins JP, Richardson AD, Braswell BH, Ollinger SV, Hollinger DY, Smith ML (2007) Refining light-use efficiency calculations for a deciduous forest canopy using simultaneous tower-based carbon flux and radiometric measurements. *Agric Meteorol* 143(1–2):64–79

- Kayet N, Pathak K, Chakrabarty A, Sahoo S (2016) Spatial impact of land use/land cover change on surface temperature distribution in Saranda Forest Jharkhand. *Model Earth Syst Environ* 2(3):127
- Kayet N, Pathak K, Chakrabarty A, Singh CP, Chowdary VM, Kumar S, Sahoo S (2019) Forest health assessment for geo-environmental planning and management in hilltop mining areas using Hyperion and Landsat data. *Ecol Ind* 106:105471
- Kayet N, Pathak K, Chakrabarty A, Kumar S, Chowdary VM, Singh CP, Basumatary S (2019) Assessment of foliar dust using hyperion and landsat satellite imagery for mine environmental monitoring in an open cast iron ore mining areas. *J Clean Product* 218:993–1006
- Ke LIU, Qing-bo ZHOU, Wen-bin WU, Tian XIA, Hua-jun TANG (2016) Estimating the crop leaf area index using hyperspectral remote sensing. *J integrative agriculture* 15(2):475–491
- Kruse FA, Boardman JW, Huntington JF (1999) Fifteen years of hyperspectral data: Northern grapevine mountains, Nevada. In: *Proceedings of the 8th JPL Airborne earth science workshop: Jet Propulsion Laboratory Publication, JPL Publication*, pp 99–117
- Kumar K, Singh NM, Kerr JM (2015) Decentralisation and democratic forest reforms in India: moving to a rights-based approach. *Forest Policy Econ* 51:1–8
- Lee KS, Cohen WB, Kennedy RE, Maiersperger TK, Gower ST (2004) Hyperspectral versus multispectral data for estimating leaf area index in four different biomes. *Remote Sens Environ* 91(3–4):508–520
- Li Z, Guo X (2016) Remote sensing of terrestrial non-photosynthetic vegetation using hyperspectral, multispectral, SAR, and LiDAR data. *Prog Phys Geogr* 40(2):276–304
- Loret F, Peñuelas J, Ogaya R (2004) Establishment of co-existing Mediterranean tree species under a varying soil moisture regime. *J Veg Sci* 15(2):237–244
- Ma J, Sun DW, Qu JH, Pu H (2017) Prediction of textural changes in grass carp filets as affected by vacuum freeze drying using hyperspectral imaging based on integrated group wavelengths. *LWT-Food Sci Technol* 82:377–385
- Mashimbye ZE, Cho MA, Nell JP, De Clercq WP, Van Niekerk A, Turner DP (2012) Model-based integrated methods for quantitative estimation of soil salinity from hyperspectral remote sensing data: a case study of selected South African soils. *Pedosphere* 22(5):640–649
- Navinkumar TU, Parmar SK (2016) Unmixing of hyperpectral image using nonlinear parametric model. In: *2016 IEEE international conference on recent trends in electronics, information & communication technology (RTEICT)*, IEEE, pp 1206–1211
- Pathak VN (2016) Development of an atmospheric correction method for retrieval of surface reflectance from satellite data. *Doctoral dissertation, Sardar Patel University*
- Peddle DR, Boulton RB, Pilger N, Bergeron M, Hollinger A (2008) Hyperspectral detection of chemical vegetation stress: evaluation for the Canadian HERO satellite mission. *Can J Remote Sens* 34(sup1):S198–S216
- Petropoulos GP, Vadrevu KP, Kalaitzidis C (2013) Spectral angle mapper and object-based classification combined with hyperspectral remote sensing imagery for obtaining land use/cover mapping in a Mediterranean region. *Geocarto Int* 28(2):114–129
- Plaza A, Valencia D, Plaza J, Chang CI (2006) Parallel implementation of endmember extraction algorithms from hyperspectral data. *IEEE Geosci Remote Sens Lett* 3(3):334–338
- Rodríguez-Pérez JR, Riaño D, Carlisle E, Ustin S, Smart DR (2007) Evaluation of hyperspectral reflectance indexes to detect grapevine water status in vineyards. *Am J Enology and Viticulture* 58(3):302–317
- Serrano L, Penuelas J, Ustin SL (2002) Remote sensing of nitrogen and lignin in Mediterranean vegetation from AVIRIS data: decomposing biochemical from structural signals. *Remote Sens Environ* 81(2-3):355–364
- Sims DA, Gamon JA (2002) Relationships between leaf pigment content and spectral reflectance across a wide range of species, leaf structures and developmental stages. *Remote Sens Environ* 81(2-3):337–354
- Thenkabail PS (2001) Optimal hyperspectral narrow bands for discriminating agricultural crops. *Remote Sens Rev* 20(4):257–291

- Thenkabail PS, Enclona EA, Ashton MS, Van Der Meer B (2004) Accuracy assessments of hyperspectral waveband performance for vegetation analysis applications. *Remote Sens Environ* 91(3-4):354–376
- Tuominen J, Lipping T, Kuosmanen V (2008) Assessment of ENVI forest health tool in detection of dust and seepage contaminated forest areas. In: IGARSS 2008–2008 IEEE international geoscience and remote sensing symposium, Vol 3. IEEE, pp. III–1358
- Tuominen J, Lipping T, Kuosmanen V, Haapanen R (2009) Remote sensing of forest health. In: Ho P-GP (ed) *Geoscience and remote sensing*. InTech, Shanghai, China, pp 29–52
- Vauhkonen J, Mehtätalo L, Packalén P (2011) Combining tree height samples produced by airborne laser scanning and stand management records to estimate plot volume in Eucalyptus plantations. *Can J Res* 41(8):1649–1658
- Wang W, Lawrence KC, Ni X, Yoon SC, Heitschmidt GW, Feldner P (2015) Near-infrared hyperspectral imaging for detecting Aflatoxin B1 of maize kernels. *Food Control* 51:347–355
- Wilson JW (1981) Analysis of growth, photosynthesis and light interception for single plants and stands. *Ann Bot* 48(4):507–512
- Zarco-Tejada PJ, Berni JA, Suárez L, Sepulcre-Cantó G, Morales F, Miller JR (2009) Imaging chlorophyll fluorescence with an airborne narrow-band multispectral camera for vegetation stress detection. *Remote Sens Environ* 113(6):1262–1275
- Zarco-Tejada PJ, Guillén-Climent ML, Hernández-Clemente R, Catalina A, González MR, Martín P (2013) Estimating leaf carotenoid content in vineyards using high resolution hyperspectral imagery acquired from an unmanned aerial vehicle (UAV). *Agric for Meteorol* 171:281–294
- Zarco-Tejada PJ, Miller JR, Mohammed GH, Noland TL, Sampson PH (2002) Vegetation stress detection through chlorophyll a+ b estimation and fluorescence effects on hyperspectral imagery. *J Environ Qual* 31(5):1433–1441
- Zarco-Tejada PJ, Ustin SL, Whiting ML (2005) Temporal and spatial relationships between within-field yield variability in cotton and high-spatial hyperspectral remote sensing imagery. *Agron J* 97(3):641–653